JOURNAL OF MATERIALS SCIENCE 26 (1991) 3165–3170

Grain-boundary sliding measurements in Al_2O_3 by machine vision photogrammetry

C. R. BLANCHARD, R. A. PAGE
Southwest Research Institute, San Antonio, TX 78228-0510, USA

The nucleation, growth and coalescence of grain-boundary cavities is the primary damage mechanism observed during creep of structural ceramics. Furthermore, grain-boundary sliding (GBS) has been identified as the driving force process. Although the creep characteristics of structural ceramics have been extensively studied, very little is known about the details of GBS during creep and how GBS relates to cavitation kinetics. This paper presents the results of a study using a machine vision system to measure Mode II GBS displacements in a Lucalox Al_2O_3. Specifically, sliding displacements as large as 0.4 μm were measured. The measured displacements indicate that some grain boundaries experienced shear strains and strain rates of 4200% and $2.3 \times 10^{-2}\,s^{-1}$, respectively. The techniques utilized for these measurements are described in detail, and data gathered during a $2\frac{1}{2}$ h compressive creep test under a stress of 138 MPa at 1600 °C are presented and discussed.

1. Introduction

The increased interest in ceramics for use as elevated-temperature structural components has resulted in a need to understand high-temperature damage mechanisms. The creep properties of polycrystalline Al_2O_3 have been widely studied [1–8], and the prominent damage mechanism has been observed to be the stress-induced nucleation, growth and coalescence of cavities on grain boundaries, eventually leading to crack formation and failure [4–6, 8]. Furthermore, it has been concluded that grain-boundary sliding (GBS), whereby stress concentrators arise at various critical points on the grain boundaries (particles, ledges and triple points) providing a high enough stress for cavity nucleation to occur, is a critical component in the damage process. Assuming stochastic grain-boundary sliding, Page and Chan [9, 10] have developed a model that provides information regarding the relationships between GBS and cavity nucleation, growth and coalescence. However, due to the complications involved, actual GBS measurements of ceramic materials are scarce, and when available, are often only qualitative or relative in nature [11, 12]. This absence of useful GBS data certainly hinders our ability to predict accurately damage accumulation and failure during high-temperature creep of ceramics.

The GBS measurement literature is primarily focused on metals and includes both polycrystalline and bi-crystal systems. Bi-crystal measurements have been performed on both metals [13] and ceramics [14, 15]. Unfortunately, bi-crystals lack the constraint that is provided by surrounding grains in polycrystalline materials. This lack of a true representation of a polycrystalline system does not allow the bi-crystal data to be particularly useful in polycrystalline-based models. The most popular technique used to measure polycrystalline GBS displacements, the line offset method, has only been applied to metal systems [16–22]. Line offset measurements require a set of linear markers, such as scratches [17, 19, 20], fiducial grids [22], secondary slip bands [16], or oxide layers [18], superimposed on the microstructure. The information made available by this technique is seemingly straightforward, but, in fact, is complicated by the fact that only a limited number of data points may be recorded (corresponding to the number of lines intersecting any given grain). It should also be noted that many of the previous efforts using the line offset method were limited to determining the contribution of GBS to the total sample elongation or to distinguishing between the GBS and the diffusional contributions to elongation. The more limited ceramics literature has focused on the grain-shape-change technique [12] and visual microstructural comparison [11] for measuring GBS. Although the cited literature does reveal some information relating GBS to specimen elongation and the various deformation components involved, quantitative details concerning GBS kinetics in ceramics are still quite scarce. There thus exists a need for further quantitative information about GBS in polycrystalline ceramics, particularly in systems for which cavitation kinetics are well characterized.

The purpose of this paper is to present a new technique developed to measure GBS displacements and strains due to creep in a polycrystalline ceramic microstructure using a machine vision photogrammetry system. The vision system is a machine-implemented version of the stereoimaging technique. Stereoimaging compares two photographs that represent displacements in one relative to the other. The in-plane displacements are perceived in the third dimension when viewed in the stereoscope and may be measured using photogrammetric techniques [23].

0022–2461/91 $03.00 + .12

Stereoimaging has been used successfully to measure displacements important in understanding the micromechanics of materials. For example, crack opening displacement measurements have been used in determining the driving force for large and small fatigue cracks [24, 25] and for cracks in the interfaces of composite materials [26]. Also, crack-tip micromechanics [27, 28] and fatigue crack closure [29] have been studied extensively using stereoimaging.

The measurements performed in this work used a machine vision system that digitized the photographic images and automated the displacement measurements. With the human visual system of the photogrammetrist, displacement is determined by observing surface features surrounding the location to be measured. The brain then assimilates this information to form a visual surface upon which the floating point of the instrument being used is placed and a measurement recorded. The image processing system of the machine vision system also observes features on one area of a digitized photograph but uses an organized search and train programme to carry out the comparison, find the closest equivalent area, and make the displacement measurements.

The technique has proved to be very powerful. Entire areas of microstructure may be observed and displacement arrays generated, thus enabling the calculation of strains, in this case, those caused by GBS during creep of a ceramic. The following will describe the application of a machine vision system to the measurement of GBS displacements and strains due to creep in a ceramic. This initial treatment will provide considerable detail of the experimental procedures due to the high degree of intricacy needed to record the measurements. Also, the results of these new measurements will be presented and discussed.

2. Experimental procedure

2.1. Material

The purpose of this study was to measure the relative in-plane grain displacements resulting from grain-boundary sliding during creep. Lucalox alumina was chosen for the creep studies due to its relatively large grains and glass-free grain boundaries, factors which together resulted in fewer complications when digitizing the microstructures. Also, previous small-angle neutron scattering (SANS) measurements have provided data on the creep cavitation kinetics in Lucalox [30, 31].

2.2. Creep tests

Compression specimens were machined into in right-circular cylinders, 1.27 cm long and 0.318 cm diameter. The ends were ground and lapped flat and parallel to within 5 μm. For the purpose of taking frequent microstructural replicas without removing the specimen, a polished flat, 1.27 cm long and 0.318 cm in diameter, was ground and lapped on the radial surface of the cylinder. The specimens were then thermally etched for 1 h at 1600 °C in air to delineate the grain boundaries. Replicas of the samples were then taken to characterize the pre-crept baseline microstructure.

Compressive creep tests were performed on the as-sintered, machined specimens under a constant stress of 137.8 MPa at 1600 °C in a titanium-gettered argon atmosphere. The creep tests were interrupted every 30 min to allow replicas to be taken, during which time a compressive stress of 114.4 MPa was maintained. The creep tests were continued for a total of $2\frac{1}{2}$ h.

2.3. Replicas

A series of microstructural replicas of the polished and etched flat surface of the creep specimen was taken after each 30-min test interval. The replicas were subsequently mounted and flattened on glass slides and coated with aluminium to enhance contrast. The coated replicas were then photographed to record the creep history of individual groups of grains. Specifically, randomly chosen areas containing a group of approximately 15 grains were photographed at a magnification of $\times 500$. Photographs of identical groups of grains taken from each of the test intervals were then used for the sliding displacement measurements.

2.4. The machine vision system

The DISMAP system (measurement of micro-displacements by machine vision photogrammetry), developed by Franke *et al.* [32] and shown schematically in Fig. 1, includes a Cognex 2000 image processing system which provides fast correlated searching for pattern matching combined with standard image processing capabilities. Photographs of identical areas at two different creep intervals were placed on stands shown on the right side of the figure under two stereo cameras. One photograph was placed on a fixed stage and used as a reference while the second photograph was placed on the x, y, θ translation/rotation stage. Two cameras fed images of the photographs to the Cognex 2000 machine vision system where they were digitized and saved for further processing. The image processor was interactive with a video display monitor, an ASCII graphics terminal, and a DEC VAX 11/780 mainframe computer. The operator communicated through the use of the graphics terminal and the trackball. The connection to the main frame computer allowed the measured displacements to be processed and presented graphically.

2.5. Displacement measurements

Initially, the DISMAP system was calibrated by imaging a grid of known spacing and indicating its coordinates with the trackball. Then, the two photographs were placed on their respective stages and aligned with an anagraphic stereoviewing concept where one image is seen in red and the other in green. The fine alignment was then accomplished by setting the computer to the "flicker" mode where the images were alternately displayed on the video screen with a rapidity of from 200–400 ms. This procedure allows

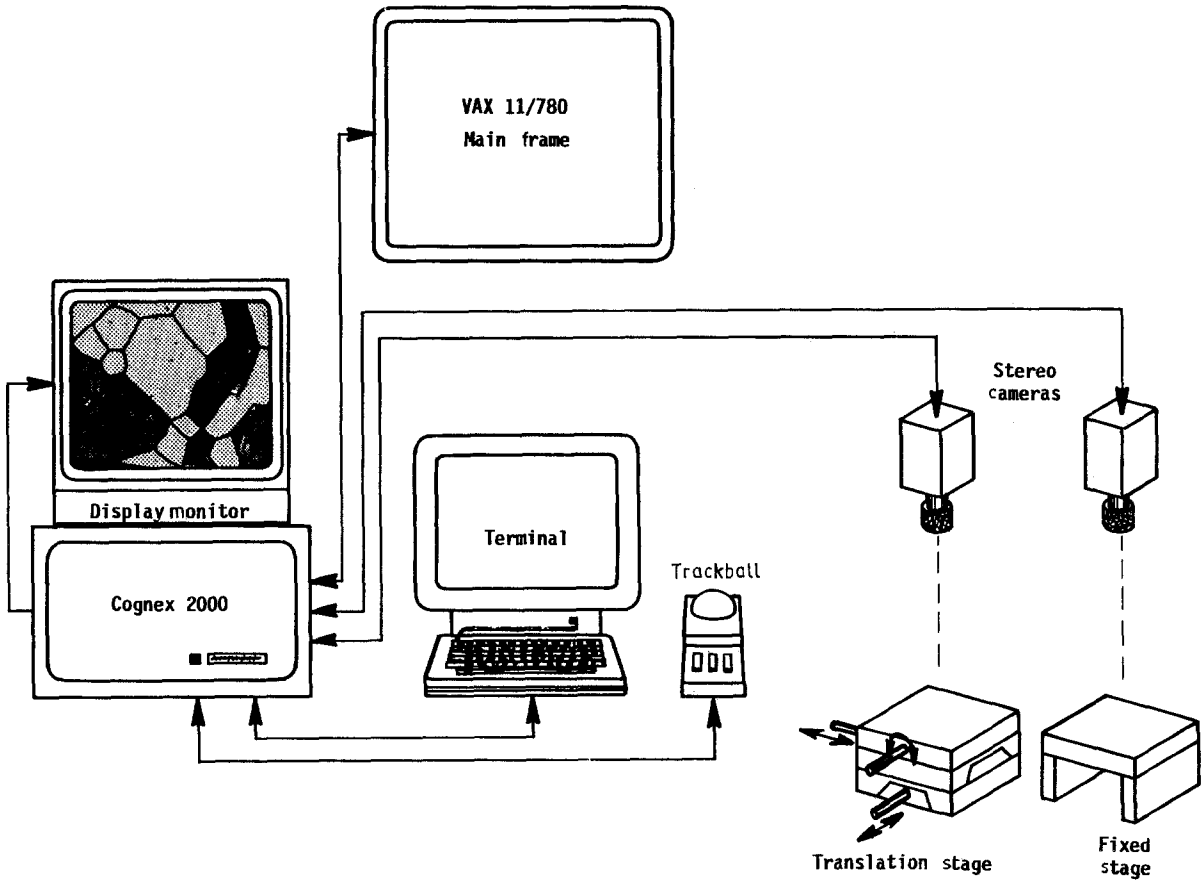

Figure 1 Schematic diagram of the DISMAP machine vision system.

for more refined alignment of the images and location of the point of zero displacement, the point of reference by which all displacements are measured. The photographs were always oriented with the grain boundary vertical on the graphics screen such that displacements measured in the x-direction represented Mode I opening of the boundary, while y-displacements represented Mode II shear. During the alignment process, the F-stops were adjusted on the imaging lenses to ensure optimum light level and contrast, and the focus was checked.

In preparation for data acquisition, the photograph magnification was specified, and a grid, like that seen in Fig. 2, was superimposed on the image to specify the points at which measurements were to be made (the nodes of the grids). For the GBS measurements, the grid was centred across one grain boundary and spacings were chosen to give optimum viewing clarity. The origin of the grid was specified at the grain boundary for easy location of the grain boundary in the graphical presentations.

Following the calibration, alignment and grid set-up procedures, displacement measurements were performed through a training and search sequence. Both the training and search areas are square areas of pixels centred around each grid node, and their size is specified by the operator. In general, the training area should be set large enough so as to include enough features for the image processing system to discriminate the chosen area from other nearby areas, yet small enough not to overlap with adjacent areas. The search area is adjusted based on a combination of factors including the training area chosen and the magnitude of the displacements expected.

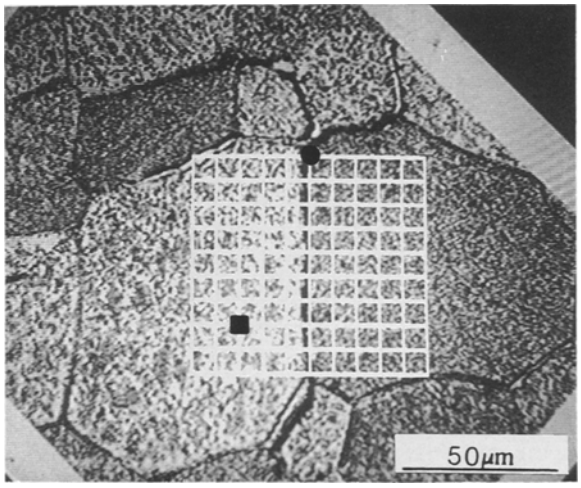

Figure 2 Example of a grid placed on a grain pair to provide points of reference for displacement measurements. Note the origin (●) was chosen at the grain boundary and the point of zero displacement (■) was chosen in the lower left corner.

Once the displacements had been measured, they were displayed superimposed on the grain pair of interest for direct viewing of the relative grain movements, as shown in Fig. 3. The general trend of the displacement vectors obtained with the DISMAP system was verified by placing the two photographs in a stereoviewer and orienting the grain boundary in question parallel to the viewer's eyes to observe shear displacement, and perpendicular to observe opening

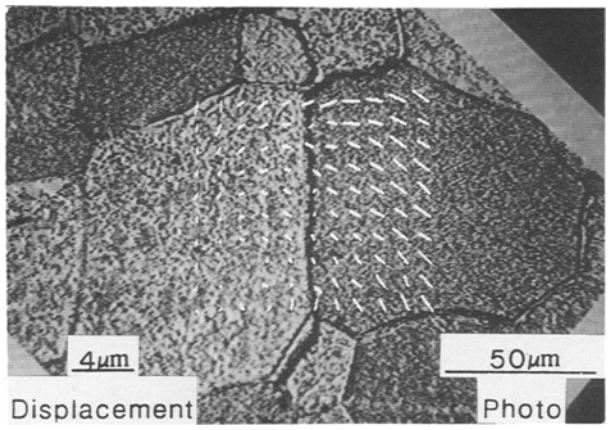

Figure 3 Example of a displacement field superimposed on the grain pair showing the movement measured with respect to the point of zero displacement (lower left corner).

displacement. For more detailed information on the DISMAP system and its limitations, see [32].

3. Results and discussion

The results of the machine vision displacement measurements for a typical grain pair are shown in Fig. 3. Each displacement vector originates from a point corresponding to a grid node and describes both the magnitude and direction of the displacement measured at that point relative to the chosen point of zero displacement. The vector field may be observed to exhibit some discontinuities, for example, in the grain boundary itself, where thickening of the boundary due to continued thermal etching can confuse the recognition system, and along outer extremities where other features such as adjacent grain boundaries and other sliding grains may enter into the search field and also confuse the recognition system. Displacement vectors within the individual grains, however, were considered to provide an accurate representation of the displacements of their respective grid nodes.

Measurement of the in-plane displacements of two adjacent grains permits the determination of the sliding displacement along the grain boundary by simply determining the relative displacement of the grain pair in the direction of the grain boundary. By initially placing the y-axis of the displacement grid parallel to the grain boundary of interest, a simplified situation exists in which the relative y-displacement of the grain pair corresponds to the sliding displacement along the grain boundary. Similarly, the relative x-displacement corresponds to relative motion perpendicular to the grain boundary. However, because the angle that the grain boundary makes with the surface plane is not known, it is not possible to determine, from the in-plane displacements alone, whether the measured x-displacement represents a Mode I type opening of the boundary, an out of plane sliding, or some combination of the two. Due to the ambiguity in the interpretation of the x-displacements, only the y-displacements will be dealt with in the subsequent discussion. Efforts to develop a means of using the x-displacements along with measured z-displacements are underway, however.

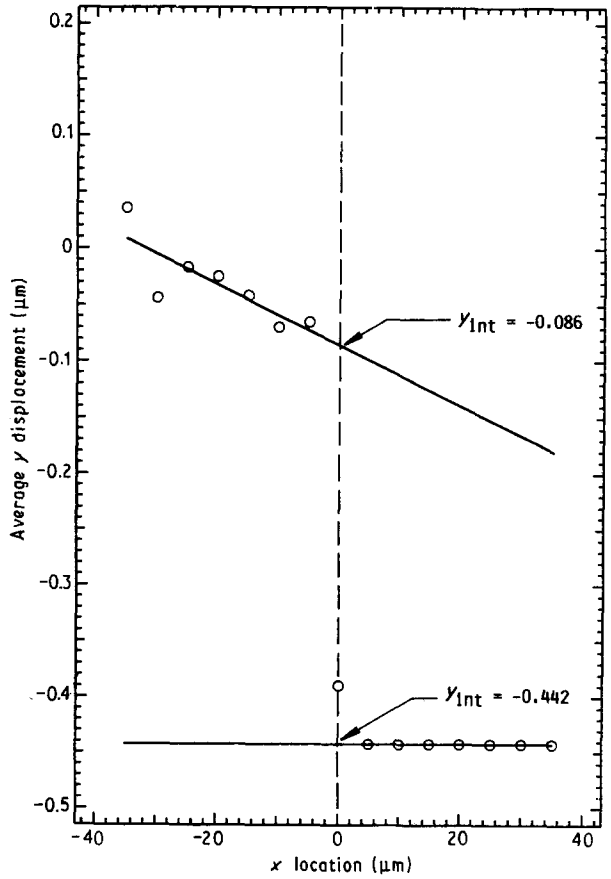

Figure 4 The average y-displacement versus the x-location across a grain pair showing the relative GBS displacement at the grain boundary ($x = 0$).

The measured y-displacements were used to determine the shear displacement between the two grains in the following manner. The displacement, d_y, was plotted versus the x location for a number of rows of vectors. These curves, which were generally overlapping, were averaged together and a least squares linear approximation was performed on the resulting array of points in each grain (Fig. 4). When plotted in this manner, the difference between the d_y ($x = 0$) values for each of the two grains represents the total shear displacement between the grains. It should be noted that the method of data analysis described above provides for an unambiguous determination of the average rigid body shear displacement that took place across the grain boundary. Normal strains within the grains were so small that they had no effect on the sliding determination, and shear strains and rigid body rotations affect only the slope of the curve and not the value of d_y obtained at the boundary.

Figs 4 and 5 show representative d_y versus x plots for two different Lucalox grain pairs. A 0.36 μm shear displacement is evident for the grain boundary in Fig. 4. In contrast, the grain boundary measured in Fig. 5 exhibited no measurable sliding displacement. Small shear strains or rigid body rotations were present in both cases, as evinced by the nonzero slope displayed by one of the grains in each of the two figures. These results indicate that the machine vision based measurement system is capable of differentiating sliding boundaries from nonsliding boundaries and providing a quantitative measurement of the total sliding displacement that occurred within a given time period.

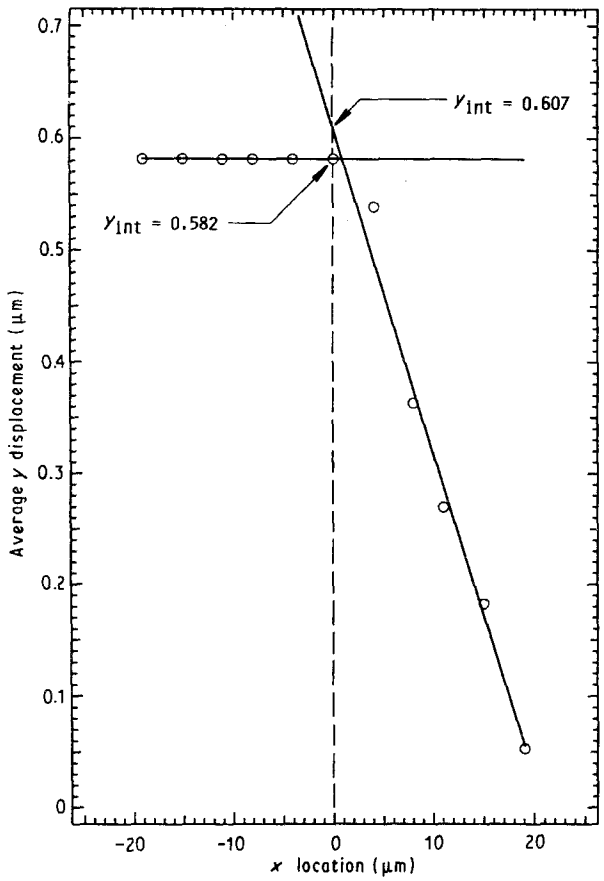

Figure 5 The average y-displacement versus the x-location across the grain boundary showing minimal GBS displacement at a grain pair ($x = 0$).

The shear strain accumulated within a sliding boundary may be estimated from the grain-boundary thickness and the amount of relative displacement between grains. The grain-boundary thickness in Lucalox was given by Carter *et al.* [33] as 8.5 nm, which with a boundary shear displacement of 0.36 μm, as measured in Fig. 4, yields a calculated GBS shear strain of 4200%. This strain accumulated in a 30 min time interval during the creep test. The average strain rate is therefore calculated to be $2.3 \times 10^{-2}\,s^{-1}$ for this grain boundary.

Initially, a strain of 4200% and a strain rate of $2.3 \times 10^{-2}\,s^{-1}$ appear to be very high for grain-boundary sliding in a polycrystalline ceramic. However, if one considers the small grain-boundary volume in relation to the total specimen size and the fact that a large percentage of the 20% strain to failure of Lucalox during creep under these conditions occurs by grain-boundary sliding, it seems reasonable that one grain boundary could experience the seemingly large reported strain and strain rate.

In making measurements of relatively small displacements, such as those reported here, the question of accuracy and reproducibility arises. Franke *et al.* [32] performed accuracy measurements on the machine vision system and determined the system accuracy to be better than 0.20 pixels, or approximately 40 μm on the photograph. For the × 500 photographs used in this study, a 0.20 pixel accuracy corresponds to a system accuracy of ≈ 0.08 μm. Of course, other factors outside of the system may influence the overall accuracy such as the quality of the photograph and any human error induced during alignment.

4. Conclusion

It has been shown that a machine vision system can be successfully used to measure Mode II GBS displacements in a compressively crept Lucalox specimen. The measurements performed thus far indicate that the degree of sliding varies from boundary to boundary, with some grains exhibiting no measurable sliding, while others exhibited shear strains and strain rates above 4000% and $2 \times 10^{-2}\,s^{-1}$, respectively. These measurements are on-going and are ultimately planned to encompass measurement of the angular and time dependence of the boundary shear displacements and a determination of the percentage of grain boundaries that are actively sliding during any given time interval. The successful collection of these data is expected to allow comparisons with cavitation data and promote a better understanding of the relationship between GBS, cavitation, and failure. Although Lucalox alumina is a relatively coarse-grained ceramic, similar measurements should be possible in finer grained materials by using higher magnification photomicrographs.

References

1. R. L. COBLE and Y. H. GUERARD, *J. Amer. Ceram. Soc.* **46** (1963) 353.
2. A. H. HEUER, R. M. CANNON Jr and N. J. TIGHE, in "Ultrafine-grain ceramics", edited by J. J. Burke, N. L. Reed and V. Weiss (Syracuse University Press, Syracuse, NY, 1970) pp. 339–65.
3. A. MOCELLIN and W. D. KINGERY, *J. Amer. Ceram. Soc.* **54** (1971) 339.
4. J. R. PORTER, W. BLUMENTHAL and A. G. EVANS, *Acta Metall.* **29** (1981) 1899.
5. B. J. DALGLEISH, E. B. SLAMOVICH and A. G. EVANS, *J. Amer. Ceram. Soc.* **68** (1985) 575.
6. K. JAKUS, S. M. WIEDERHORN and B. J. HOCKEY, *ibid.* **69** (1986) 725.
7. A. H. CHOKSHI and J. R. PORTER, *J. Mater. Sci.* **21** (1986) 705.
8. R. A. PAGE, J. LANKFORD, K. S. CHAN, K. HARDMAN-RHYNE and S. SPOONER, *J. Amer. Ceram. Soc.* **70** (1987) 137.
9. R. A. PAGE and K. S. CHAN, *Met. Trans.* **18A** (1987) 1843.
10. K. S. CHAN and R. A. PAGE, *J. Mater. Sci.* **20** (1990) 4622.
11. T. SUGITA and J. A. PASK, *J. Amer. Ceram. Soc.* **53** (1970) 609.
12. W. R. CANNON and O. D. SHERBY, *ibid.* **60** (1977) 44.
13. T. WATANABE and P. W. DAVIES, *Phil. Mag. A* **37** (1978) 649.
14. M. A. ADAMS and G. T. MURRAY, *J. Appl. Phys.* **33** (1962) 2126.
15. P. F. BECHER and H. PALMOUR III, *J. Amer. Ceram. Soc.* **53** (1970) 119.
16. D. McLEAN, *J. Inst. Metals* **80** (1951–52) 507.
17. B. FAZAN, O. D. SHERBY and J. E. DORN, *Trans. AIME J. Metals* August **6** (1954) 919.
18. Y. ISHIDA, A. W. MULLENDORE and N. J. GRANT, *Trans. Met. Soc. AIME* **233** (1965) **204**.
19. E. H. AIGELTINGER, *J. Mater. Sci.* **9** (1974) 644.
20. T. G. LANGDON, D. SIMPSON and R. C. GIFKINS, *Acta Metall.* **31** (1983) 939.
21. T. WATANABE, *Met. Trans.* **14A** (1983) 531.
22. K. READING and D. A. SMITH, *Phil. Mag. A* **51** (1985) 71.

23. H. M. KARRARA (ed.), "Handbook of Non-Topographic Photogrammetry" (American Society of Photogrammetry Falls Church, Va, 1979).
24. D. L. DAVIDSON, *Acta Metall.* **36** (1988) 2275.
25. *Idem.*, in "Fatigue crack growth under variable amplitude loading", edited by J. Petit, D. Davidson, S. Suresh and P. Rabbe (Elsevier Science, Essex, 1988) pp. 1–11.
26. K. S. CHAN and D. L. DAVIDSON, *Engng Fract. Mech.* **33** (1989) 451.
27. D. L. DAVIDSON and J. LANKFORD, *Mater. Sci. Engng* **74** (1985) 189.
28. D. L. DAVIDSON, *Engng Fract. Mech.* **25** (1986) 123.
29. D. L. DAVIDSON and J. LANKFORD, *Mater. Sci. Engng* **60** (1983) 225.
30. R. A. PAGE and J. LANKFORD, *J. Amer. Ceram. Soc.* **66** (1983) C-146.
31. R. A. PAGE, J. LANKFORD and S. SPOONER, *J. Mater. Sci.* **19** (1984) 3360.
32. E. A. FRANKE, D. J. WENZEL and D. L. DAVIDSON, *Rev. Sci. Inst.* (1991) in press.
33. C. B. CARTER, D. L. KOHLSTEDT and S. L. SASS, *J. Amer. Ceram. Soc.* **63** (1980) 623.

Received 29 November 1989
and accepted 13 August 1990